ACADEMIA ROMÂNĂ

Revue Roumaine de Chimie

http://web.icf.ro/rrch/

Rev. Roum. Chim., **2018**, *63*(4), 321-336

COMPUTATIONAL STUDIES ON THE SELF-REACTION MECHANISM OF THE SIMPLEST CRIEGEE INTERMEDIATE CH_2OO

Wen-Mei Wei,[a,*,†] Qia Xu,[a,†] Ren-Hui Zheng[b,*] and Yi-De Qin[b,*]

[a] College of Basic Medicine, Anhui Medical University, Hefei, Anhui 230032, China
[b] Beijing National Laboratory for Molecular Sciences, State Key Laboratory for Structural Chemistry of Unstable and Stable Species, Institute of Chemistry, Chinese Academy of Sciences, Zhongguancun, Beijing 100190, China

Received November 21, 2017

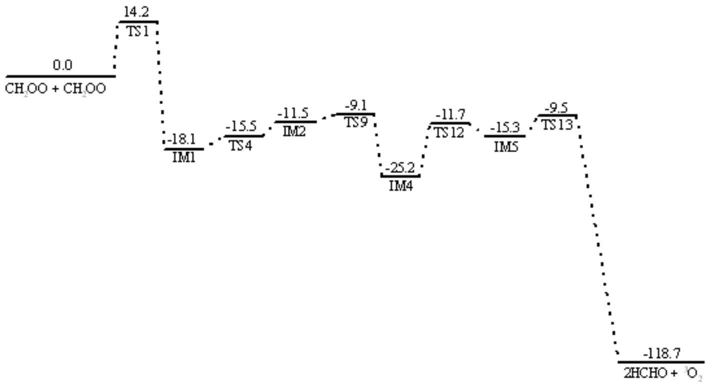

The famous Criegee intermediates play important roles in atmospheric chemistry. The self-reaction of the simplest Criegee intermediate, CH_2OO, is an important loss pathway for CIs in many current laboratory experiments where CH_2OO concentrations are high and need to be investigated both experimentally and theoretically to probe its kinetics and detailed mechanisms. To provide insight into the reaction mechanism of CH_2OO self-reaction, stationary points on the complex potential energy surfaces of CH_2OO + CH_2OO have been searched at the CCSD(T)/AUG-cc-pVTZ//B3LYP/AUG-cc-pVTZ level of theory. The geometries and relative energies for various stationary points are determined. The theoretical results indicate that there is a reaction path for the self-reaction of CH_2OO producing the final products, two HCHO plus $^3O_2$. This is a new alternative mechanism with the small Gibbs free energy barrier of 14.2 kcal/mol and the Gibbs free energy of the overall process is -118.7 kcal/mol. Though the barriers of these reactions are higher than those of the primary reaction path in literature [Nat. Chem. **6**, 477 (2014)] that is the most feasible path. The reaction can also occur easily in atmosphere.

INTRODUCTION

The famous Criegee intermediates (CI, RR'COO, often called carbonyl oxides) are formed by the reaction of ozone (O_3) with alkenes in the atmosphere[1,2] and play important roles in atmospheric chemistry[3,4] because they are not only the intermediates of the alkene ozonolysis, but also the OH sources, the oxidants for NO_2 and SO_2, and possibly other donations to tropospheric chemistry.[5] Extensive experimental and theoretical investigations have been carried out on CIs after their first postulated in 1949 by Rudolf Criegee. [6] However, because of lacking appropriate detection methods, the characteristic of CIs has been hampered for a long time and most of the information obtained experimentally was highly indirect [5] until recently, when the direct detection of the gaseous CIs was reported. [7-11]

The simplest CI, CH_2OO (formaldehyde oxide) is produced in the atmosphere from the reaction of O_3 with ethene (C_2H_4) and a number of 1-alkenes via formation and fragmentation of alkene ozonide, [12] was first detected by Taatjes *et al.* in 2008. [7] In the gas phase, the chemically activated CH_2OO^* may either undergo unimolecular decomposition

[*] Corresponding authors: cherrywwm@ustc.edu (W.-M. Wei), zrh@iccas.ac.cn (R.-H. Zheng), qinyide@hotmail.com (Y.-D. Qin)

[†] These authors have contributed equally to this work.

reactions to produce the stable products such as HCHO, CO, CO_2, H_2O and HCOOH [13] or be collisionally stabilized with the bath gas to generate the longer-lived stabilized Criegee intermediate (SCI) [14,15] which undergoes further reactions with other molecules, such as NO_2,[13] H_2O,[8] SO_2.[8, 16-17]

Vereecken *et al.* said that a lot reactions of CI are still poorly understood, but are significant for the explanation of experimental data, both in laboratory and in the field. [5] Su *et al.* [10] experimentally detected CH_2OO loss on the order of microseconds using the infrared observation of CI and they suggested that this decay is dominated by fast CI self-reactions driven by the relatively high CH_2OO concentrations. Thus the self-reaction of CH_2OO can be an important loss pathway for CIs in many current laboratory experiments where CH_2OO concentrations are high [18,19] and needs to be investigated both experimentally and theoretically to probe its kinetics and mechanisms.

Some studies have been carried out on the self-reaction of CH_2OO. Vereecken *et al.*[5] have theoretically investigated the potential energy surface (PES) of this reaction at the CCSD(T)//M06-2X level of theory. And using variational Transition State Theory (TST), they reported a rate coefficient of $\geq 4 \times 10^{-11}$ cm^3 $molecule^{-1}$ s^{-1} at the temperature of 300 K for it in 2014. [5] Moreover, they recommend that this self-reaction be further studied by experimental means and even higher levels of theoretical methodologies. [5] Su *et al.* [12] calculated the PES of this reaction at CCSD(T)//B3LYP/AUG-cc-pVTZ-pp level. They found that the self-reaction of CH_2OO was extremely rapid, and the rate coefficient (k_{self}) is estimated to be $(4 \pm 2) \times 10^{-10}$ cm^3 $molecule^{-1}$ s^{-1} at 343 K using transient IR absorption spectroscopy. [12] However, about half a year later, the same group reported that the dependence of k_{self} on temperature is expected to be small, so the value of $k_{self} = (4 \pm 2) \times 10^{-10}$ cm^3 $molecule^{-1}$ s^{-1} at 343 K reported previously might have been overestimated and their final determination of k_{self} is $(8 \pm 4) \times 10^{-11}$ cm^3 $molecule^{-1}$ s^{-1} at 295 K. [20] In 2014, Buras *et al.* [19] reported that they can accurately determine absolute CH_2OO concentrations using laser flash photolysis and the accurately k_{self} they measured is $(6.0 \pm 2.1) \times 10^{-11}$ cm^3 $molecule^{-1}$ s^{-1} at 297 K. Chhantyal-Pun *et al.* [18] recently reported a rate coefficient of $k_{self} = (7.35 \pm 0.63) \times 10^{-11}$ cm^3 $molecule^{-1}$ s^{-1} at 293 K using cavity ring-down spectroscopy.

All these researches indicate the self-reaction of CH_2OO is fast and a more detailed mechanism of this reaction still needs to be established. Furthermore, just as Vereecken *et al.* said that theoretical analysis plays a significant role in our understanding of CIs. [5] Thus, in this work, we investigated the complicate potential energy surface of $CH_2OO + CH_2OO$ reaction theoretically and tried our best to elucidate its reaction mechanism.

COMPUTATIONAL DETAILS

The geometries of all the studied structures were optimized using the density functional theory (B3LYP) [21,22] combined with the Dunning basis set AUG-cc-pVTZ (denoted as B3LYP/AUG-cc-pVTZ). [23,24] Harmonic vibrational frequencies and the corresponding zero-point vibrational energies (ZPE) were obtained at the same level of theory, and scaled by a factor of 0.96. [25] In the following discussion, reaction intermediates are labeled as IM and transition states as TS. Intrinsic reaction coordinate (IRC) [26] computations at the same level were carried out to ensure that the transition states connect the right reactants and products. The electronic energies were improved by coupled-cluster theory CCSD(T)[27] on the B3LYP geometries, employing AUG-cc-pVTZ Dunning basis set (denoted CCSD(T)/AUG-cc-pVTZ). The corrected relative Gibbs free energies (named $G_{CCSD(T)/AUG\text{-}cc\text{-}pVTZ}$, in the unit of kcal/mol) are applied in the following energy discussion unless special explanation. And the correction is: $G_{CCSD(T)/AUG\text{-}cc\text{-}pVTZ} = E_{CCSD(T)/AUG\text{-}cc\text{-}pVTZ} + [G_{B3LYP/AUG\text{-}cc\text{-}pVTZ} - E_{B3LYP/AUG\text{-}cc\text{-}pVTZ}]$. Furthermore, the temperature is taken as 298.15 K and the pressure is 1 atm when the Gibbs free energy is calculated.

Both Vereecken *et al.*[5] and Su *et al.*[12] have reported a barrierless reaction path for the self-reaction of CH_2OO to form a six-membered ring intermediate (see IM 15 in Fig. 1). We scanned the potential energy surface of this combining reaction using the M06-2X density functional [28] with AUG-cc-pVTZ basis set to optimize the geometries of the species on the PES and CCSD(T)/AUG-cc-pVTZ method to calculate the corresponding energies. The two C—O bonds were shortened at the same time when we scanned the formation PES of IM 15 from the reactants $2CH_2OO$. When the two CH_2OO molecules are far away from each other, the intermolecular interactions between them have been considered. Thus at this computation, we used M06-2X theory instead of B3LYP method because M06-2X works better on the intermolecular interactions between the molecules than B3LYP does. There are two C—O bonds, thus theoretically it is needed to scan two-dimension potential surface, which is very time-consuming. To simplify the problem, we assumed that the two C—O bonds change at the same distance. Hence, we obtained the one-dimension potential surface along the C—O bond. All the calculations were done using Gaussian 09 software.[29]

RESULTS AND DISCUSSION

The self-reaction of CH_2OO proceeds with six pathways (including 26 paths) leading to products in this study. Figure 1 shows the optimized geometries of stationary points on the CH_2OO + CH_2OO potential energy surface. The relative electronic energies and Gibbs free energies calculated at different level of theory are listed in Table 1. The T1 diagnostic values of the species involved in the studied PES obtained at the CCSD(T)/AUG-cc-pVTZ level of theory are listed in Table 2. Most T1 values are in the range of 0.01 to 0.04. Generally speaking, the T1 values above 0.044 are regarded to produce unreliable results.[30]

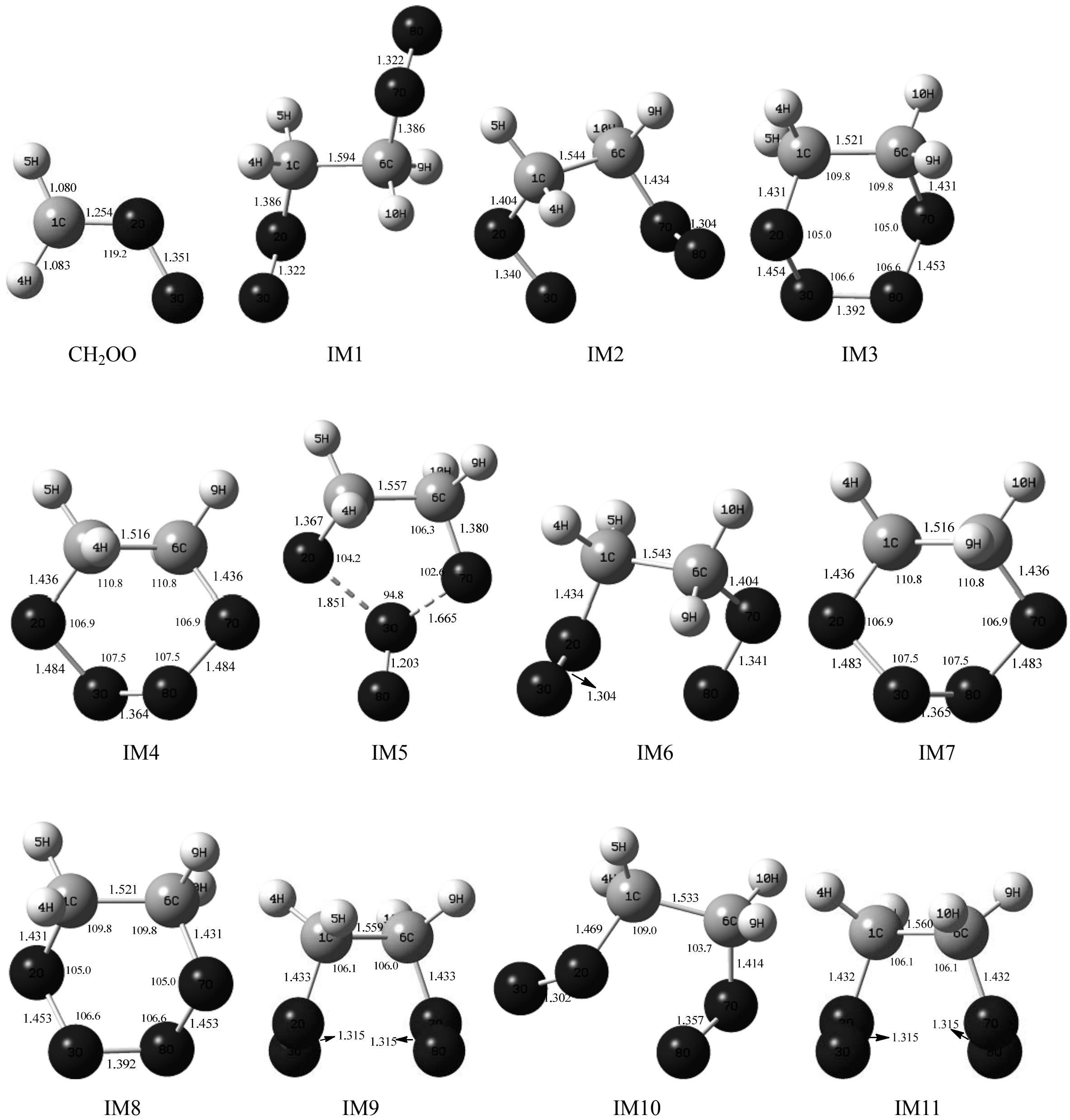

Fig. 1 – Geometric parameters of related molecules on the CH_2OO + CH_2OO energy surface at B3LYP/AUG-cc-pVTZ level of theory. Bond lengths are in angstroms, bond angles are in degrees.

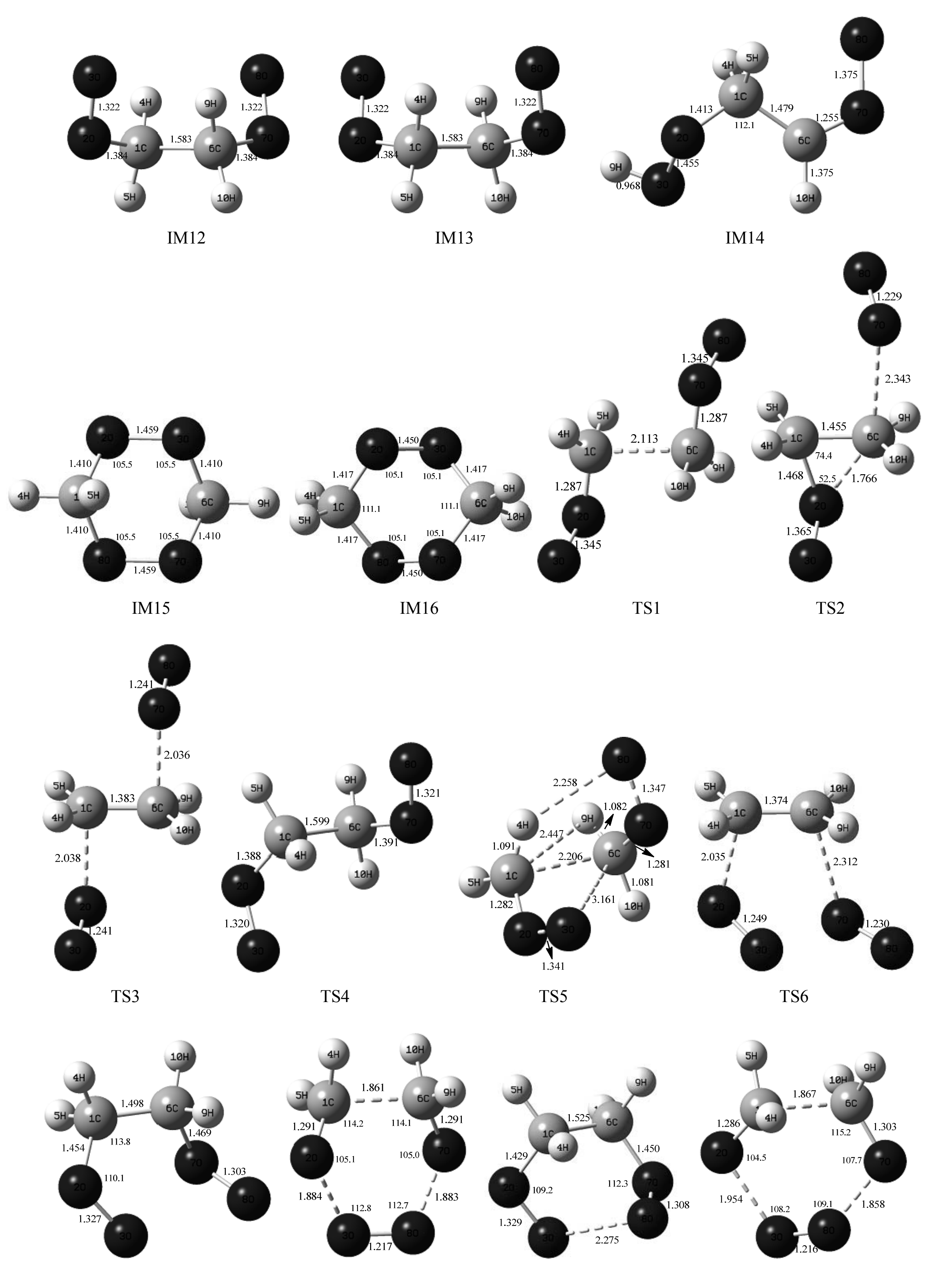

Fig. 1 – Continued.

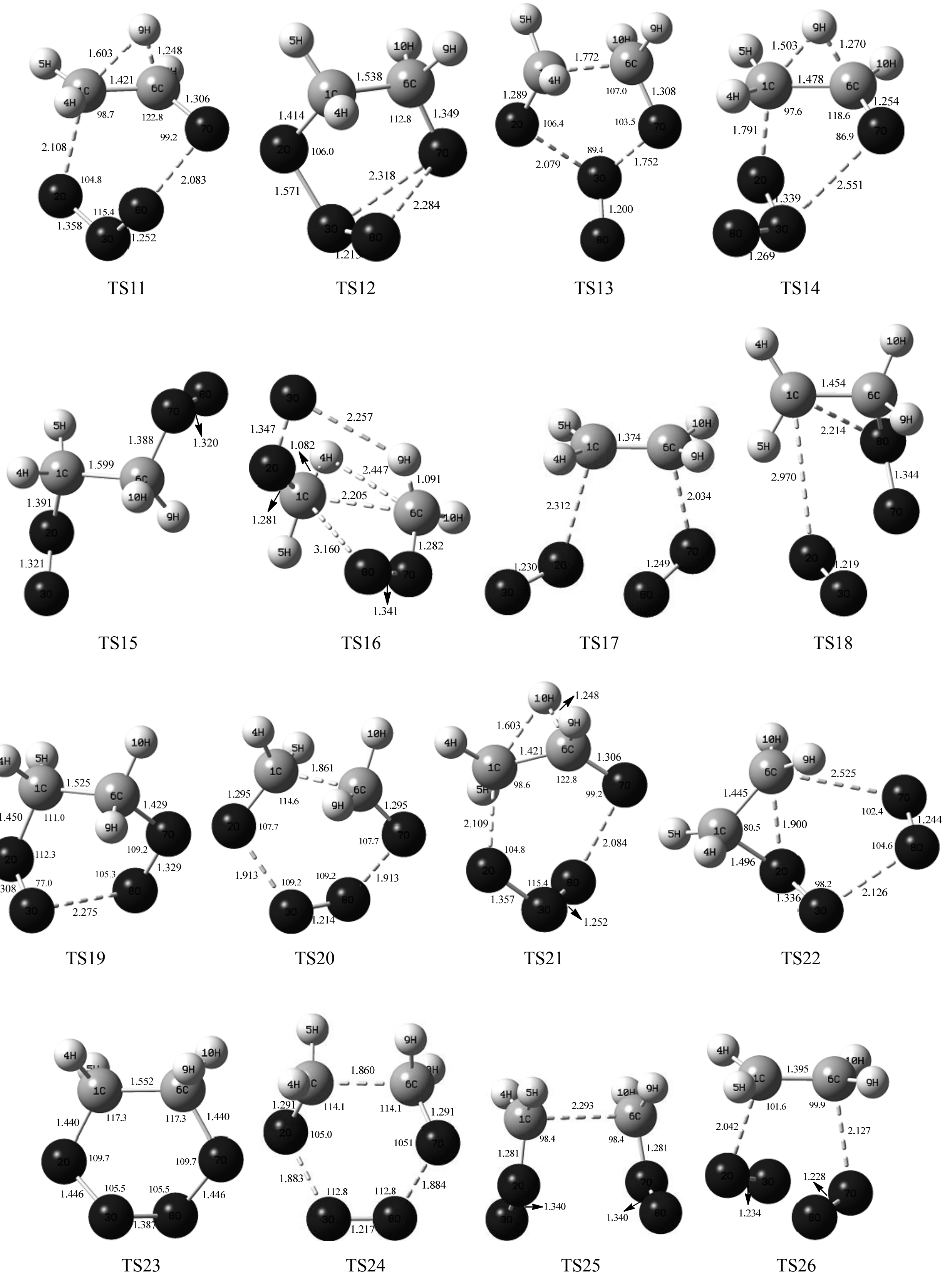

Fig. 1 – Continued.

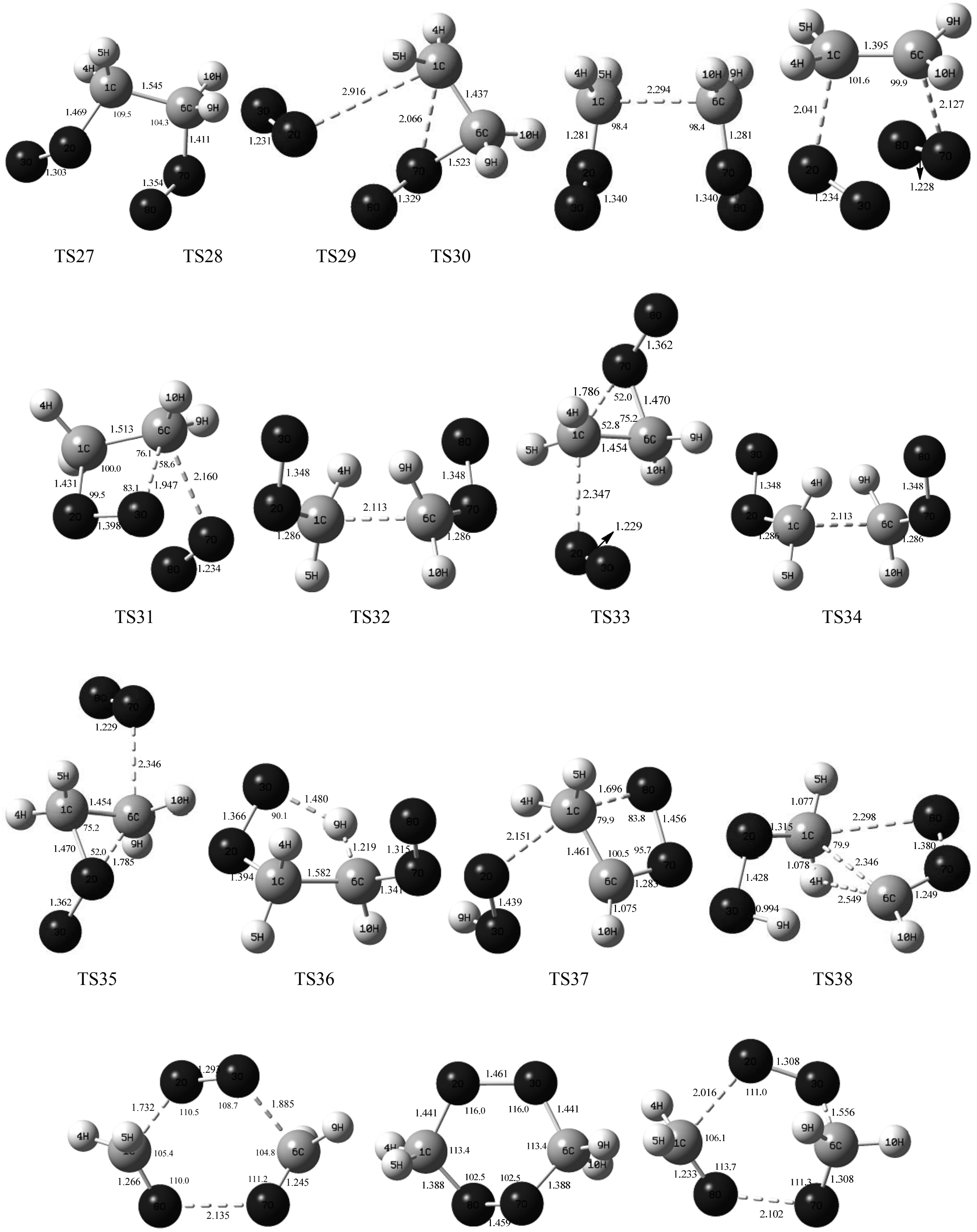

TS27 TS28 TS29 TS30

TS31 TS32 TS33 TS34

TS35 TS36 TS37 TS38

TS39 TS40 TS41

Fig. 1 - Continued.

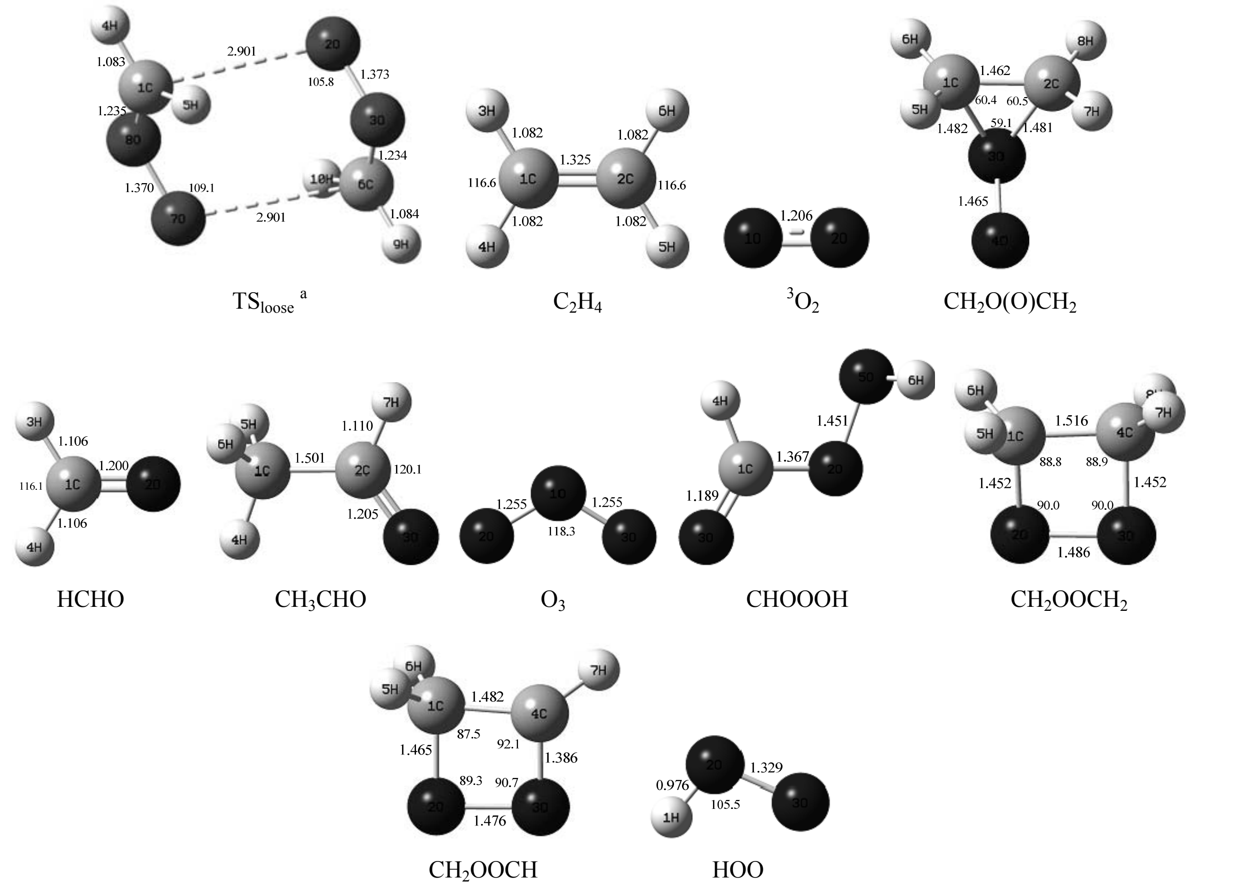

Fig. 1 – Geometric parameters of related molecules on the $CH_2OO + CH_2OO$ energy surface at B3LYP/AUG-cc-pVTZ level of theory. Bond lengths are in angstroms, bond angles are in degrees.

Table 1

Imaginary frequencies (IF, in cm^{-1}) of the transition states, zero-point vibrational energies (ZPE, in kcal/mol), entropy S (in cal mol^{-1} K^{-1}), relative energies (RE1, in kcal/mol) and Gibbs free energies (ΔG1, in kcal/mol) at 298.15K of the reactants, intermediates, transition states and products calculated at B3LYP/AUG-cc-pVTZ level

Species	B3LYP/AUG-cc-pVTZ					CCSD(T)/AUG-cc-pVTZ	
	IF	ZPE [a]	S	RE1	ΔG1	RE2 [b]	ΔG2 [c]
$CH_2OO + CH_2OO$		37.4	119.1	0.0	0.0	0.0	0.0 [d]
IM1		40.8	82.4	-5.0	8.8	-35.2	-18.1
IM2		41.4	75.7	-13.9	2.1	-31.4	-11.5
IM3		42.1	71.7	-44.3	-26.9	-53.9	-31.8
IM4		41.8	73.9	-36.4	-19.7	-46.2	-25.2
IM5		40.7	76.4	-22.4	-7.2	-33.8	-15.3
IM6		41.4	75.7	-13.9	2.1	-31.4	-11.5
IM7		41.8	73.9	-36.4	-19.7	-46.2	-25.2
IM8		42.1	71.7	-44.3	-26.9	-53.9	-31.8
IM9		41.9	74.6	-16.3	0.4	-33.4	-12.2
IM10		41.5	76.3	-11.1	4.8	-25.6	-5.6
IM11		41.9	74.6	-16.3	0.4	-33.4	-12.2
IM12		40.8	78.2	-8.2	6.6	-33.0	-14.7
IM13		40.8	78.2	-8.2	6.6	-33.0	-14.7
IM14		40.5	80.9	-53.8	-39.7	-59.9	-42.7
IM15		43.3	70.8	-87.6	-68.9	-98.5	-73.9
IM16		42.8	72.2	-79.1	-61.1	-89.9	-66.5
TS1	-318.6	39.0	83.7	2.0	13.7	1.0	14.2
TS2	-325.2	38.1	86.7	35.6	45.8	31.1	42.0
TS3	-340.4	37.1	88.9	39.3	48.3	38.1	46.7
TS4	-89.0	40.7	76.3	-3.4	11.6	-33.8	-15.5
TS5	-293.5	39.0	80.3	2.1	14.7	-0.4	13.7

Table 1 (continued)

TS6	-264.8	38.6	79.2	22.0	34.5	9.3	23.0
TS7	-242.8	40.6	74.9	3.7	18.9	-29.3	-11.0
TS8	-712.1	38.8	77.4	-15.6	-2.6	-19.1	-4.8
TS9	-268.2	41.1	72.6	-8.0	8.2	-29.0	-9.1
TS10	-767.5	38.5	79.0	-9.8	2.5	-14.3	-0.9
TS11	-1064.8	37.1	77.4	25.0	36.3	22.0	33.0
TS12	-565.3	39.4	74.2	-4.2	10.0	-27.7	-11.7
TS13	-533.3	38.9	77.7	-19.5	-6.4	-24.1	-9.5
TS14	-1061.3	37.2	77.6	13.1	24.4	8.6	19.6
TS15	-89.1	40.7	76.3	-3.4	11.6	-33.8	-15.5
TS16	-293.7	39.0	80.3	2.1	14.7	-0.4	13.7
TS17	-265.4	38.6	79.2	22.0	34.5	9.3	23.0
TS18	-325.8	37.6	86.3	43.0	52.8	28.0	37.9
TS19	-268.4	41.1	72.6	-8.0	8.2	-29.0	-9.1
TS20	-768.3	38.3	75.1	-9.5	3.4	-13.6	0.2
TS21	-1064.8	37.1	77.4	25.0	36.3	22.0	33.0
TS22	-251.5	38.4	80.6	31.9	43.9	25.6	38.5
TS23	-258.7	41.7	72.8	-31.4	-14.8	-40.0	-19.1
TS24	-711.9	38.8	77.4	-15.6	-2.6	-19.1	-4.7
TS25	-258.8	39.0	79.6	3.6	16.4	1.0	15.4
TS26	-417.9	38.8	80.0	22.3	34.7	8.2	22.1
TS27	-65.5	41.5	72.0	-11.1	5.6	-25.5	-4.8
TS28	-289.4	37.8	83.7	35.2	45.9	28.7	39.8
TS29	-258.9	39.0	79.6	3.6	16.4	1.0	15.4
TS30	-418.4	38.8	80.0	22.3	34.7	8.2	22.1
TS31	-685.3	39.7	76.6	28.9	42.9	24.8	41.1
TS32	-324.8	39.2	79.0	-0.3	12.7	-2.9	11.9
TS33	-316.2	38.0	87.9	35.8	45.7	31.2	41.7
TS34	-324.9	39.2	79.0	-0.3	12.7	-2.9	11.9
TS35	-316.4	38.0	87.9	35.8	45.7	31.2	41.7
TS36	-878.5	38.7	75.2	-3.4	9.7	-13.3	1.1
TS37	-510.8	39.2	78.9	-0.1	13.0	-4.8	10.0
TS38	-421.3	38.9	78.2	9.4	22.3	6.7	21.0
TS39	-550.0	38.0	80.9	-31.0	-19.5	-34.9	-22.9
TS40	-331.5	42.4	71.5	-70.3	-52.7	-79.8	-57.1
TS41	-416.1	38.3	78.9	-27.4	-15.1	-37.6	-24.5
TS_{loose} [e]	-51.2	39.2	81.4	-12.5	-1.1	-10.5	1.9
$C_2H_4 + 2\ ^3O_2$		35.1	153.0	-42.7	-53.9	-39.2	-52.6
$CH_2O(O)CH_2 + {}^3O_2$		38.4	114.2	-5.0	-2.5	-7.7	-4.3
$2HCHO + {}^3O_2$		34.2	156.2	-102.7	-115.6	-102.5	-118.7
$CH_3CHO + O_3$		37.6	120.9	-48.2	-48.3	-55.3	-55.2
HCHO + CHOOOH		37.8	120.9	-139.2	-138.9	-143.2	-142.5
$CH_2OOCH_2 + {}^3O_2$		39.5	114.4	-48.2	-44.8	-52.5	-47.1
CH_2OOCH + HOO		37.5	120.1	-2.9	-3.1	-3.9	-4.1

[a] Scaled by a factor of 0.96.[25]
[b] The relative energies are obtained at CCSD(T)/AUG-cc-pVTZ level.
[c] The corrected relative Gibbs free energy.
$G2 = E_{CCSD(T)/AUG\text{-}cc\text{-}pVTZ} + [G_{B3LYP/AUG\text{-}cc\text{-}pVTZ} - E_{B3LYP/AUG\text{-}cc\text{-}pVTZ}] + ZPE$
[d] The total Gibbs free energy is -378.589400 Hartree.
[e] IF, ZPE, S, RE1 and ΔG1 values are computed by M06-2X/AUG-cc-pVTZ method.

Table 2

The T1 diagnostic values of the reactants, intermediates, transition states and products for the self-reaction of CH_2OO using CCSD(T)/AUG-cc-pVTZ//B3LYP/AUG-cc-pVTZ method

CH_2OO	IM1	IM2	IM3	IM4	IM5	IM6	IM7
0.0435	0.0315	0.0258	0.0182	0.0184	0.0363	0.0258	0.0183
IM8	IM9	IM10	IM11	IM12	IM13	IM14	IM15
0.0182	0.0158	0.0267	0.0158	0.0271	0.0271	0.0307	0.0153
IM16	TS1	TS2	TS3	TS4	TS5	TS6	TS7
0.0148	0.0450	0.0487	0.0331	0.0294	0.0431	0.0594	0.0297
TS8	TS9	TS10	TS11	TS12	TS13	TS14	TS15

Table 2 (continued)

0.0501	0.0311	0.0508	0.0440	0.0488	0.0556	0.0267	0.0294
TS16	TS17	TS18	TS19	TS20	TS21	TS22	TS23
0.0430	0.0595	0.0734	0.0311	0.0440	0.0440	0.0397	0.0175
TS24	TS25	TS26	TS27	TS28	TS29	TS30	TS31
0.0501	0.0412	0.0467	0.0263	0.0560	0.0412	0.0467	0.0358
TS32	TS33	TS34	TS35	TS36	TS37	TS38	TS39
0.0438	0.0348	0.0438	0.0348	0.0337	0.0323	0.0339	0.0410
TS40	TS41	TS_{loose} [a]	C_2H_4	$^3O_2$	$CH_2O(O)CH_2$	HCHO	CH_3CHO
0.0147	0.0433	0.0380	0.0107	0.0176	0.0191	0.0154	0.0144
O_3	CHOOOH	CH_2OOCH_2	CH_2OOCH	HOO			
0.0265	0.0172	0.0132	0.0204	0.0302			

[a] The values are obtained at CCSD(T)/AUG-cc-pVTZ//M06-2X/AUG-cc-pVTZ level.

Pathway A

For clarity, we divide Pathway A into two parts, Pathway A (a) and Pathway A (b).

Pathway A (a)

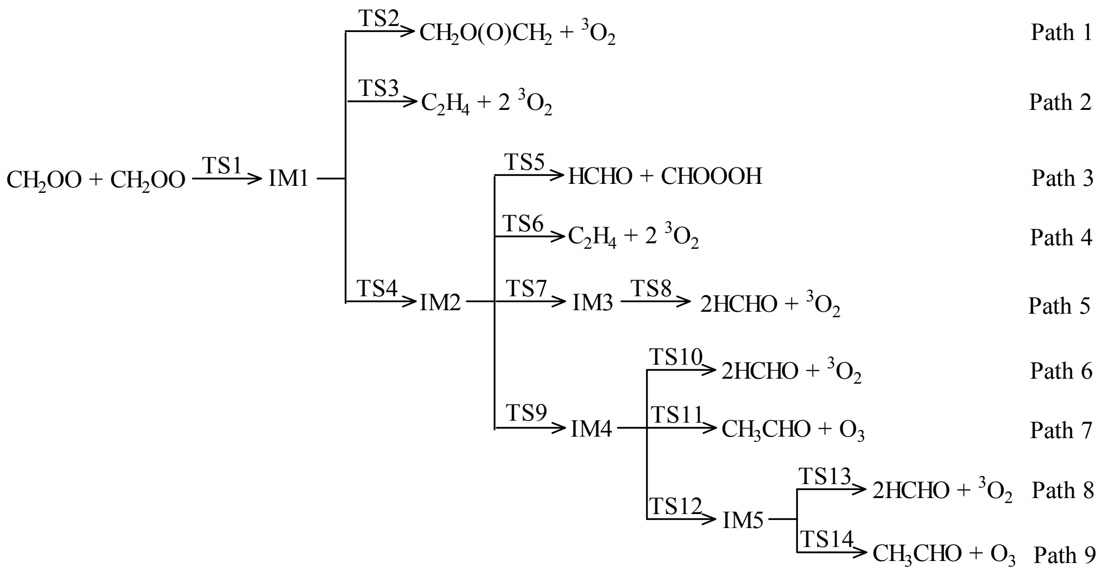

The potential energy diagram for Pathway A (a) is depicted in Fig. 2.

In this pathway, two CH_2OO molecules firstly combine to an intermediate IM1 via a transition state TS1 with an imaginary frequency of 318.6 cm^{-1}. In the structure of TS1, the forming C1…C6 distance is shortened to 2.113 Å. The Gibbs free energy barrier of this combination reaction is only 14.2 kcal/mol and indicates that it is easy to form IM1. Then from IM1, nine different paths have been studied and among them, the minimal energy path (Path 8) has been marked with the bold lines in Figure 2. Path 8 is also the lowest energy path in this study, which proceeds via several intermediates and transition states to form the final products two HCHO and $^3O_2$ in which the latter represents O_2 in its ground $^3\Sigma_g^-$ state. The other paths in this Pathway are unimportant because of the higher barriers involved. Thus we only discuss Path 8 in detail. The next step in this path is that IM1 isomerizes to IM2 via TS4 with a small imaginary frequency of 89.0 cm^{-1} and a lower barrier of 2.6 kcal/mol. This process is the C6H9H10O7O8 group in IM1 rotating around the C1—C6 bond. Note that the Gibbs free energy of TS4 is abnormally 4.0 kcal/mol lower than IM2. Then we check the electronic energies of them. As listed in Table 1, the electronic energies of TS4 and IM2 obtained at CCSD(T)/AUG-cc-pVTZ level are -33.8 and 31.4 kcal/mol, respectively. Thus the electronic energy of TS4 is only 2.4 kcal/mol lower than that of IM2 at this level of theory, which may be caused by the calculation inaccuracy. Furthermore, IRC calculations have confirmed that TS4 indeed connects IM1 and IM2. Subsequently, over a six-membered ring transition state TS9 with a low barrier of 2.4 kcal/mol and an imaginary frequency of 268.2 cm^{-1}, IM2 isomerizes to a six-membered ring intermediate IM4. In the structure of TS9, the forming O3…O8 distance is reduced to 2.275 Å. Then IM4 isomerizes to a five-membered ring intermediate IM5 via TS12 with an imaginary frequency of 565.3 cm^{-1}. The barrier of this reaction is 13.5 kcal/mol. In the structure of TS12, the forming O3…O7 distance is shortened to 2.318 Å, while the breaking O7—O8 bond is lengthened to 2.284 Å. The last step in this path is IM5 dissociating to the final products two HCHO plus $^3O_2$ via a five-membered ring transition state TS13 with an imaginary frequency of 533.3 cm^{-1}. This concerted three-bond breaking reaction has a low barrier of 5.8 kcal/mol. The breaking C1—C6, O2—O3 and O3—O7 bonds in the geometry of TS13 are stretched to 1.772, 2.079 and 1.752 Å, respectively. The Gibbs free energy of the overall process of Path 8 is -118.7 kcal/mol and the highest relative energy barrier of this channel is only 14.2 kcal/mol imposed by TS1, which indicates that this is a feasible channel for the self-reaction of CH_2OO.

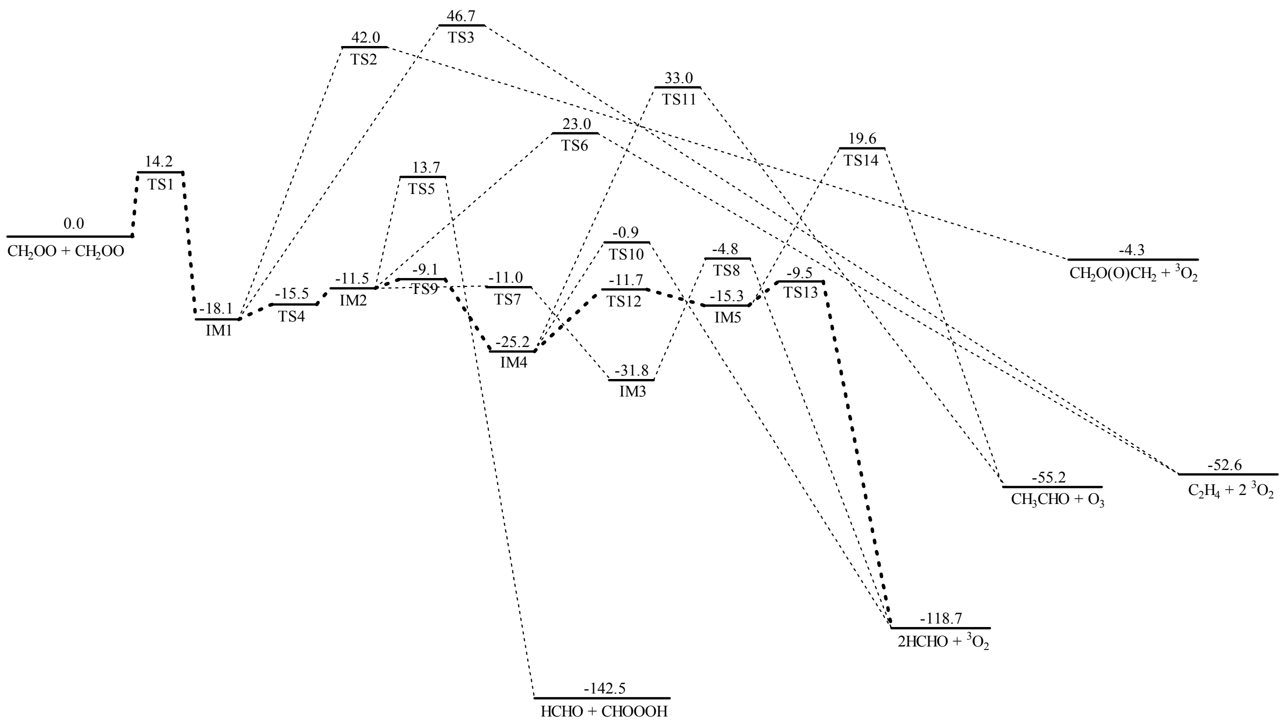

Fig. 2 – Potential energy diagram for Pathway A (a). The most feasible recombination routes are delineated in bold lines. The corrected relative Gibbs free energies are in kcal/mol.

Pathway A (b)

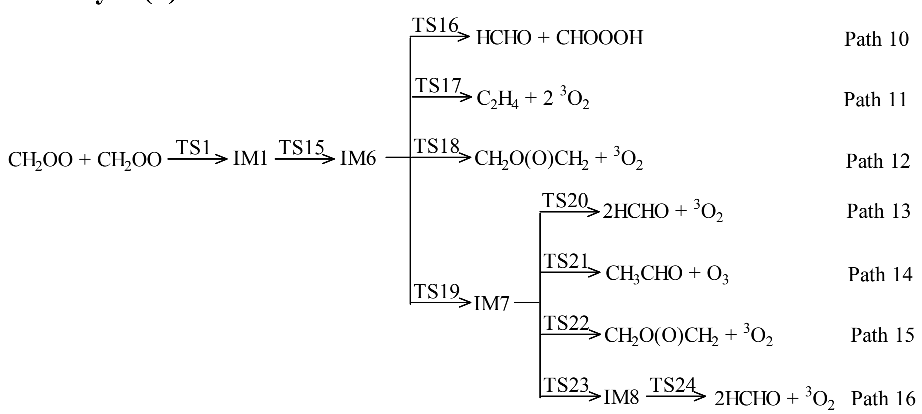

Also initiated from IM1, other seven different channels have been studied. The schematic profile of the potential energy surface for this pathway is depicted in Figure 3. Here we will discuss two competitive paths, Path 13 and Path 16, with relative lower energy barriers.

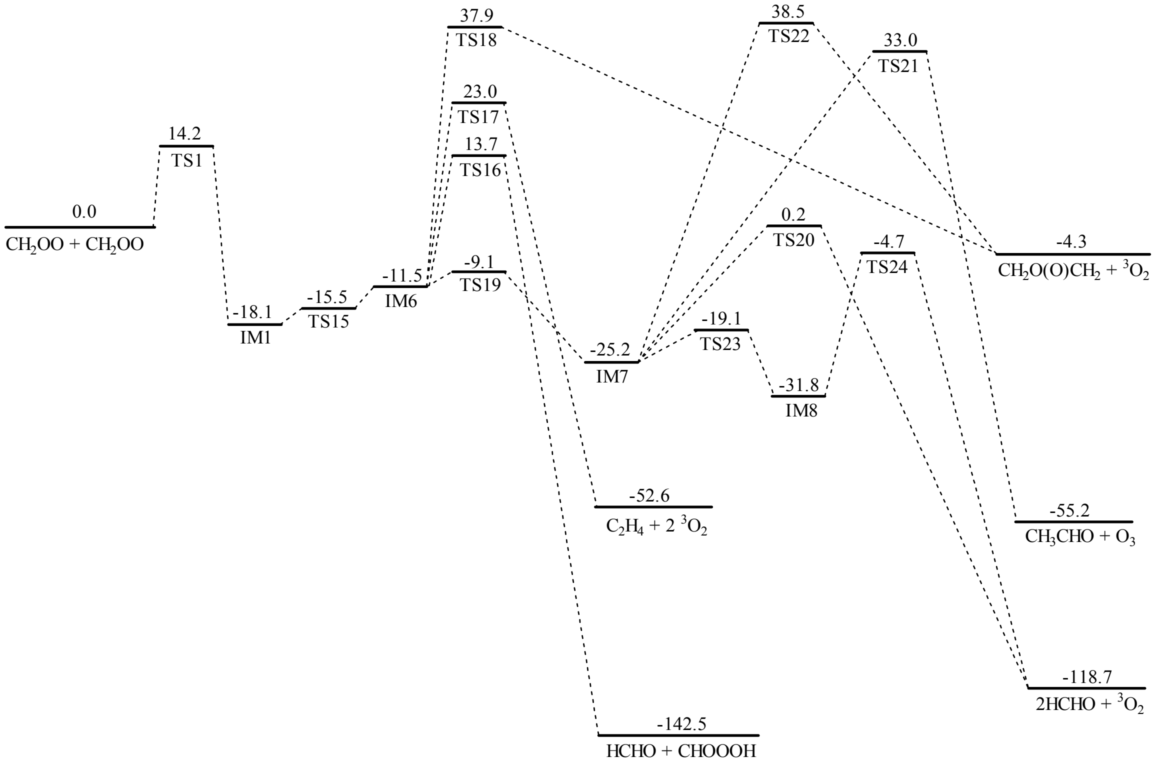

Fig. 3 – Potential energy diagram for Pathway A (b). The most feasible recombination routes are delineated in bold lines. The corrected relative Gibbs free energies are in kcal/mol.

Path 13 is the lowest energy channel in this pathway. First of all, IM1 isomerizes to IM6 via the saddle point TS15 with a small imaginary frequency of 89.1 cm^{-1} and a low barrier of 2.6 kcal/mol. This process initiates by the rotation of the C6H9H10O7O8 group in IM1 around the C1—C6 axis. Note that IM6 and IM2 discussed in Pathway A (a) are a pair of mirror image isomers. They almost have the same bond lengths and bond angles, opposite values of dihedral angles. For example, the dihedral angle among O3, O2, C1 and C6 atoms is 73.4° in IM6, while the corresponding dihedral angle among O8, O7, C6 and C1 atoms is -73.4° in IM2. And the dihedral angle among C1, C2, O7 and O8 atoms is -60.7° in IM6, while the corresponding dihedral angle among C6, C1, O2 and O3 atoms is 60.7° in IM2. Thus, this pair of mirror image isomers has the same energies from the calculated results. And like IM2, The Gibbs free energy of IM6 is abnormally 4.0 kcal/mol higher than that of TS15 because of the calculation inaccuracy. The following step is that IM6 isomerizes to IM7 through a six-membered ring saddle point TS19 with an imaginary frequency of 268.4 cm^{-1}. In the structure of TS19, the forming O3…O8 distance is reduced to 2.275 Å. The energy barrier for the formation of IM7 is 2.4 kcal/mol. The final process in this path is a concerted three-bond breaking reaction of IM7 to yield the last products, two HCHO plus $^3O_2$. The transition state of this decomposition reaction is named TS20 with a barrier of 25.4 kcal/mol and an imaginary frequency of 768.3 cm^{-1}. In the structure of TS20, the breaking C1—C6, O2—O3 and O7—O8 bonds are lengthened to 1.861, 1.913 and 1.913 Å, respectively. In a word, the highest relative energy barrier of Path 13 is 25.4 kcal/mol imposed by TS20.

Path 16 is a competitive channel with Path 13 because of the close energy barrier. The former steps of Path16 are the same to Path 13 until IM7, thus we only discuss the latter ones. IM7 can isomerize to IM8 via TS23 with a small barrier of 6.1 kcal/mol and an imaginary frequency of 258.7 cm^{-1}. Then IM8 dissociates to the final products (2HCHO+ $^3O_2$) through a six-membered ring transition state TS24 with an imaginary frequency of 711.9 cm^{-1} and a barrier of 27.1 kcal/mol. This is also a concerted three-bond breaking reaction. In the structure of TS24, the C1—C6, O2—O3 and O7—O8 bonds are stretched to 1.860, 1.883 and 1.884 Å, respectively. Thus the highest relative energy barrier of Path 16 is 27.1 kcal/mol imposed by TS24, only 1.7 kcal/mol higher than that of Path 13.

Pathway B

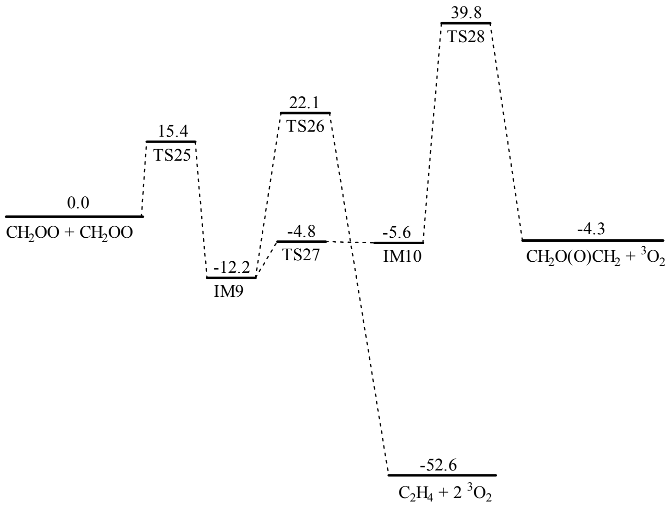

Fig. 4 – Potential energy diagram for Pathway B. The corrected relative Gibbs free energies are in kcal/mol.

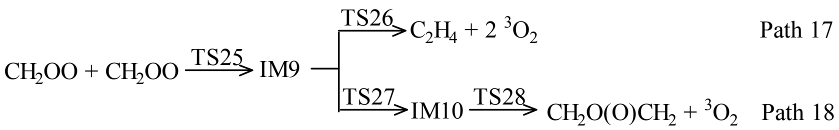

The potential energy diagram of this pathway is pictured in Figure 4, which shows that Path 17 is the lower energy one in this two channel. There are two steps in Path 17. Firstly, two CH_2OO molecules combine to form the intermediate IM9 via TS25 with an imaginary frequency of 258.8 cm^{-1} and over a barrier of 15.4 kcal/mol. In the structure of TS25, the forming C1…C6 distance is shortened to 2.293 Å. Secondly, IM9 dissociates to methane and two oxygen molecules via TS26 with an imaginary frequency of 417.9 cm^{-1}. The barrier height of this concerted bond rupture reaction is 34.3 kcal/mol. The breaking C1—O2 and C6—O7 bonds in the geometry of TS26 are lengthened to 2.042 and 2.127 Å, respectively. The overall Gibbs free energy of Path 17 is -52.6 kcal/mol and its highest relative energy barrier is 34.3 kcal/mol imposed by TS26. The high barrier suggests that this is an unfeasible channel for the self-reaction of CH_2OO.

Pathway C

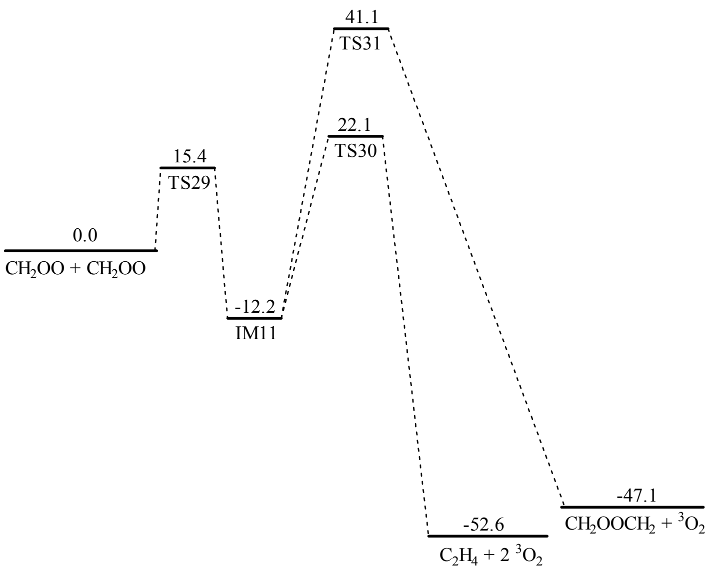

Fig. 5 – Potential energy diagram for Pathway C. The corrected relative Gibbs free energies are in kcal/mol.

$$CH_2OO + CH_2OO \xrightarrow{TS29} IM11 \xrightarrow{TS30} C_2H_4 + 2\,{}^3O_2 \qquad \text{Path 19}$$

$$IM11 \xrightarrow{TS31} CH_2OOCH_2 + {}^3O_2 \qquad \text{Path 20}$$

In this pathway shown in Figure 5, the reactants firstly associate to form IM11 over a saddle point TS29 with a barrier of 15.4 kcal/mol. The forming C1…C6 distance is shortened to 2.294 Å in the structure of TS29. Then two channels have been studied to obtain the final products from IM11, named Path 19 and Path 20, respectively. Here we discuss Path 19 because of the lower barrier height. Via TS30 with an imaginary frequency of 418.4 cm^{-1}, IM11 dissociates to C_2H_4 plus two $^3O_2$ over a barrier of 34.3 kcal/mol. In the structure of TS30, the breaking C1—O2 and C6—O7 bonds are stretched to 2.041 and 2.127 Å, respectively. The whole process of this path is similar to that of Path 17 and its highest relative energy barrier is 34.3 kcal/mol imposed by TS30.

Pathway D

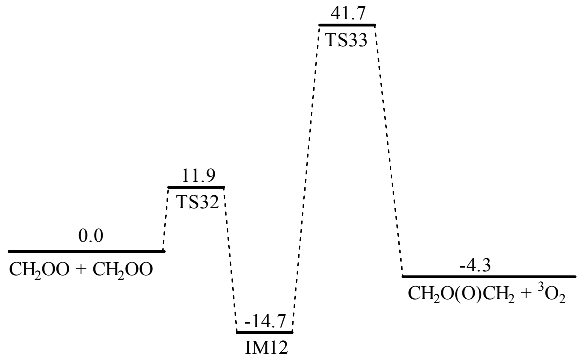

Fig. 6 – Potential energy diagram for Pathway D. The corrected relative Gibbs free energies are in kcal/mol.

$$CH_2OO + CH_2OO \xrightarrow{TS32} IM12 \xrightarrow{TS33} CH_2O(O)CH_2 + {}^3O_2 \qquad \text{Path 21}$$

Path 21 is the only channel found in Pathway D, which has been drawn in Figure 6. The relative energy barrier of this path is as high as 56.4 kcal/mol imposed by TS33, thus it is unimportant in this study.

Pathway E

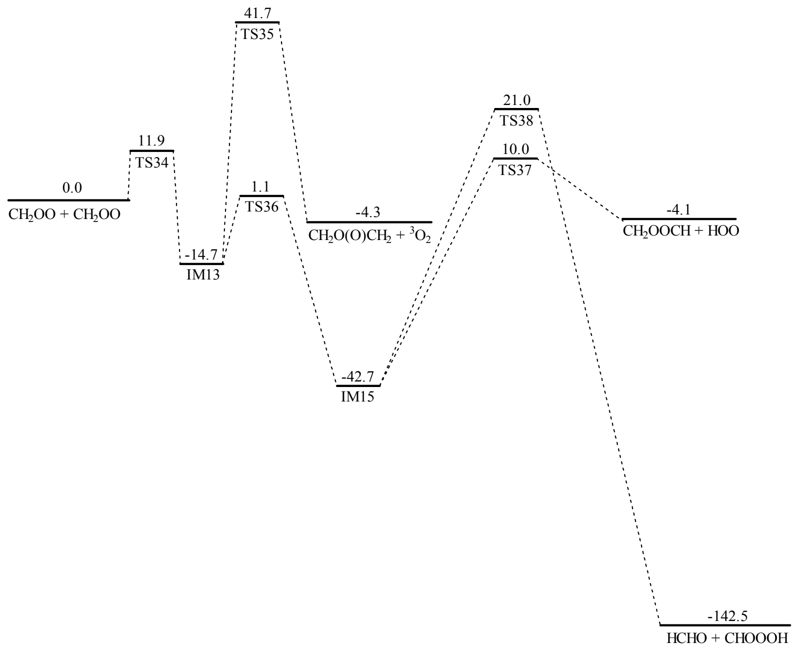

Fig. 7 – Potential energy diagram for Pathway E. The corrected relative Gibbs free energies are in kcal/mol.

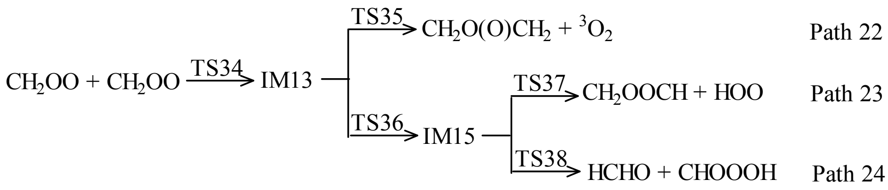

Figure 7 shows the potential energy diagram of Pathway E. There are three paths, and among them, Path 23 has the lowest energy barrier. However, the relative barrier height of this path is too high (52.7 kcal/mol imposed by TS37) to overcome, which suggests that Pathway E is an unfeasible reaction path.

Pathway F

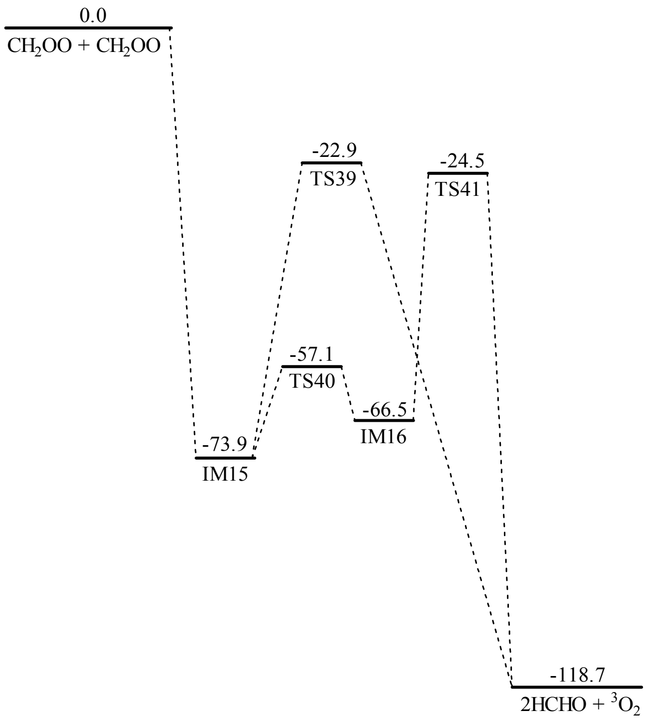

Fig. 8 – Potential energy diagram for Pathway F. The corrected relative Gibbs free energies are in kcal/mol.

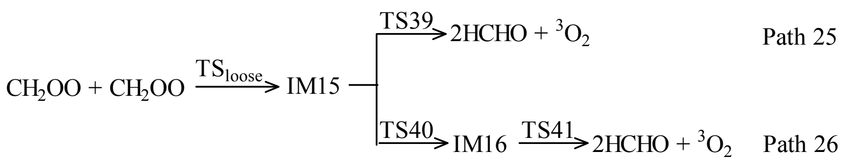

In this pathway, a new six-membered ring intermediate IM15 appears (see Figure 8), which has been reported by Vereecken *et al.*[5] at the M06-2X level of theory. They reported that the formation of the six-membered cyclic biperoxide is highly exothermic by 100.5 kcal/mol.[5] The values in Table 1 show that the formation of IM15 is exothermic by 98.5 kcal/mol at CCSD(T)/AUG-cc-pVTZ level, in good agreement with Vereecken's result. In addition, Vereecken *et al.*[5] have suggested that this process is purely attractive, without evidence for a pre-reactive complex or TS. In this study, we have also tried our best to find the transition state for the reactants to form IM15 directly, but failed. To make sure there is indeed no saddle point for the head-to-tail addition, we have scanned the formation potential energy surface of IM15 along the two C—O bonds at CCSD(T)/AUG-cc-pVTZ//M06-2X/AUG-cc-pVTZ level. The results are shown in Figure 9.

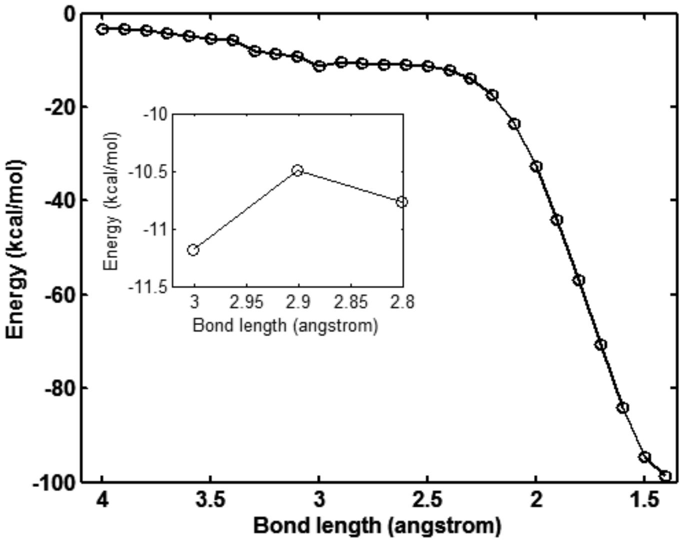

Fig. 9 – Scanning of the formation potential energy surface of IM15 from CH_2OO + CH_2OO along the two C—O bonds. The energies are calculated at CCSD(T)/AUG-cc-pVTZ//M06-2X/AUG-cc-pVTZ level.

The electronic energy of IM15 calculated at this level is -98.7 kcal/mol, agreeing very well with the -98.5 kcal/mol we obtained at CCSD(T)/AUG-cc-pVTZ level and 100.5 kcal/mol computed by Vereecken et al. [5] at M06-2X level. The total energy of the two reactant molecules CH_2OO + CH_2OO is set to be zero, and we started to scan the potential energy surface when the two C…O distances are shortened to 4.001A (the electronic energy here is -3.3 kcal/mol). Generally, with the decrease in the distances between the two carbon and oxygen atoms, the electronic energies on the potential energy surface are reduced. However, when the C1…O2 and C6…O7 distances are shortened to 2.901 Å, respectively, a saddle point named TS_{loose} appears, which is similar to a transition state. The structure of TS_{loose} is depicted in Figure 1 and its information is listed in Table 1. The electronic energy of TS_{loose} is -10.5 kcal/mol at CCSD(T)/ AUG-cc-pVTZ level, about 0.7 kcal/mol higher than the point before it. The energy barrier of the formation of IM1 in Pathway A (a) is 1.0 kcal/mol at CCSD(T)/ AUG-cc-pVTZ// B3LYP/AUG-cc-pVTZ level, only 0.3 kcal/mol higher than the barrier here. Thus we consider that both IM1 and IM15 can be produced in this reaction system.

From IM15, two channels producing formaldehyde and oxygen have been found, which are denoted as Path 25 and Path 26. The energy barrier of Path 26 is 42.0 kcal/mol imposed by TS41, and that of Path 25 is 51.0 kcal/mol imposed by TS39. Though the energy barriers are high, they are much smaller than the energy with a value of 73.9 kcal/mol when the IM15 is formed through the two CIs. This indicates that Path 25 and Path 26 are important and can be feasible to produce the product HCHO and $^3O_2$. Compared with Pathway A (a), we find that Path 25 and Path 26 can easier occur, which are primary channels. This agrees with the studies in Refs. 5 and 12.

Vereecken *et al.* have reported that the subsequent chemistry of the cyclic biperoxide (our IM15) involves chemically activated rupture of the weaker O—O bond, generating a peroxide bisalkoxy radical •OCH_2OOCH_2O•, which can remove HCHO, producing •$OOCH_2O$•, which in turn can decompose to HCHO + O_2. [5] The energy barrier of forming •OCH_2OOCH_2O• radical is 40 kcal/mol they obtained at M06-2X level,[5] which is also much smaller than IM15 forming energy. Thus we think that the corresponding path is the feasible reaction channel for the self-reaction of CH_2OO. Furthermore, Su *et al.*[12] have studied this reaction and suggested that the minimal energy path for the self-reaction of CH_2OO proceeds via $(CH_2OO)_2$ (our IM15) and a transition state to form 2HCHO plus O_2. The energy barrier they obtained at the CCSD(T)//B3LYP/aug-cc-pVTZ-pp level with corrections of vibrational ZPE is 58.1 kcal/mol, which is the Path 25 that we study and is feasible.

CONCLUSION

The calculations suggest that Path 25 and Path 26 are the most feasible channels for the self-reaction of CH_2OO to produce two HCHO plus $^3O_2$, the barrier energy forming IM15 is very small and IM15 release the energy with a value of 73.9 kcal/mol when it is generated, which is much larger than the energies needed for the following transition states TS39, TS40 and TS41.

$$CH_2OO + CH_2OO \xrightarrow{TS_{loose}} IM15 \begin{cases} \xrightarrow{TS39} 2HCHO + {}^3O_2 & \text{Path 25} \\ \xrightarrow{TS40} IM16 \xrightarrow{TS41} 2HCHO + {}^3O_2 & \text{Path 26} \end{cases}$$

The computations show that Path 8 may be the feasible channel for the self-reaction of CH_2OO to produce two HCHO plus $^3O_2$, and the Gibbs free energy of the overall process is -118.7 kcal/mol. The reactions involved in Path 8 are:

$$CH_2OO + CH_2OO \xrightarrow{TS1} IM1 \xrightarrow{TS4} IM2 \xrightarrow{TS9} IM4 \xrightarrow{TS12} IM5 \xrightarrow{TS13} 2HCHO + {}^3O_2$$

The highest Gibbs free energy barrier is 14.2 kcal/mol, imposed by TS1. Because of the small barrier heights, these reactions may also occur in atmosphere.

Acknowledgements. This work is supported by the National Natural Science Foundation of China (NSFC) (No. 21103003) and Key Project of Natural Science Research Found for Colleges and Universities in Anhui Province (No. KJ2018 A0173).

REFERENCES

1. R. Criegee, *Angew. Chem. Int. Ed. Engl.*, **1975**, *14*, 745–752.
2. S. Hatakeyama and H. Akimoto, *Res. Chem. Intermed.*, **1994**, *20*, 503–524.
3. C. A. Taatjes, O. Welz, A. J. Eskola, J. D. Savee, A. M. Scheer, D. E. Shallcross, B. Rotavera, E. P. F. Lee, J. M. Dyke, D. K. W. Mok, D. L. Osborn and C. J. Percival, *Science*, **2013**, *340*, 177–180.
4. C. A. Taatjes, D. E. Shallcross and C. Percival, *Phys. Chem. Chem. Phys.*, **2014**, *16*, 1704–1718.
5. L. Vereecken, H. Harder and A. Novelli, *Phys.Chem.Chem.Phys.*, **2014**, *16*, 4039–4049.
6. R.Criegee and G.Wenner, *Liebigs Ann. Chem.*, **1949**, *564*, 9–15.
7. C. A. Taatjes, G. Meloni, T. M. Selby, A. J. Trevitt, D. L. Osborn, C. J. Percival and D. E. Shallcross, *J. Am. Chem. Soc.*, **2008**, *130*, 11883–11885.
8. O. Welz, J. D. Savee, D. L. Osborn, S. S. Vasu, C. J. Percival, D. E. Shallcross and C. A. Taatjes, *Science*, **2012**, *335*, 204–207.
9. J. M. Beames, F. Liu, L. Lu and M. I. Lester, *J. Am. Chem. Soc.*, **2012**, *134*, 20045–20048.
10. Y.-T. Su, Y.-H. Huang, H. A. Witek and Y.-P. Lee, *Science*, **2013**, *340*, 174–176.
11. M. Nakajima and Y. J. Endo, *J. Chem. Phys.*, **2013**, *139*, 101103.
12. Y.-T. Su, H.-Y. Lin, R. Putikam, H. Matsui, M. C. Lin and Y.-P. Lee, *Nat. Chem.*, **2014**, *6*, 477–483.
13. D. Johnson and G. Marston, *Chem. Soc. Rev.*, **2008**, *37*, 699–716.
14. L. Vereecken, H. Harder and A. Novelli, *Phys. Chem. Chem. Phys.*, **2012**, *14*, 14682–14695.
15. O. Horie and G. K. Moortgat, *Atmos. Environ.*, **1991**, *25A*, 1881–1896.
16. R. L. Mauldin III, T. Berndt, M. Sipila, P. Paasonen, T. Petaja, S. Kim, T. Kurten, F. Stratmann, V. M. Kerminen and M. Kulmala, *Nature*, **2012**, *488*, 193–196.
17. T. Berndt, T. Jokinen, R. L. Mauldin, T. Petaja, H. Herrmann, H. Junninen, P. Paasonen, D. R. Worsnop and M. Sipila, *J. Phys. Chem. Lett.*, **2012**, *3*, 2892–2896.
18. C.-P. Rabi, D. Anthony, D. E. Shallcross, C. J. Percivalb and A. J. Orr-Ewing, *Phys. Chem. Chem. Phys.*, **2015**, *17*, 3617–3626.
19. Z. J. Buras, R. M. I. Elasmra and W. H. Green, *J. Phys. Chem. Lett.*, **2014**, 5, 2224–2228.
20. W.-L. Ting, C.-H. Chang, Y.-F. Lee, H. Matsui, Y.-P. Lee and J. J.-M. Lin, *J. Chem. Phys.*, **2014**, *141*, 104308.
21. A. D. Becke, *J. Chem. Phys.*, **1993**, *98*, 5648–5652.
22. C. Lee, W. Yang and R. G. Parr, *Phys. Rev. B*, **1988**, *37*, 785–789.
23. T. H. Dunning, *J. Chem. Phys.*, **1989**, *90*, 1007–1023.
24. R. A. Kendall, T. H. Dunning Jr. and R. J. Harrison, *J. Chem. Phys.*, **1992**, *96*, 6796–6806.
25. A. P. Scott and L. Radom, *J. Phys. Chem.*, **1996**, *100*, 16502–16513.
26. C. Gonzalez and H. B. Schlegel, *J. Chem. Phys.*, **1989**, *90*, 2154–2161.
27. R. J. Bartlett and G. Purvis, *Int. J. Quantum Chem.*, **1978**, *14*, 516–581.
28. Y. Zhao and D. G. Truhlar, *Theor. Chem. Acc.*, **2008**, *120*, 215–241.
29. M. J. Frisch, G. W. Trucks, H. B. Schlegel, G. E. Scuseria, M. A. Robb, J. R. Cheeseman, G. Scalmani, V. Barone, B. Mennucci, G. A. Petersson, H. Nakatsuji, M. Caricato, X. Li, H. P. Hratchian, A. F. Izmaylov, J. Bloino, G. Zheng, J. L. Sonnenberg, M. Hada, M. Ehara, K. Toyota, R. Fukuda, J. Hasegawa, M. Ishida, T. Nakajima, Y. Honda, O. Kitao, H. Nakai, T. Vreven, J. A. Montgomery, Jr., J. E. Peralta, F. Ogliaro, M. Bearpark, J. J. Heyd, E. Brothers, K. N. Kudin, V. N. Staroverov, R. Kobayashi, J. Normand, K. Raghavachari, A. Rendell, J. C. Burant, S. S. Iyengar, J. Tomasi, M. Cossi, N. Rega, J. M. Millam, M. Klene, J. E. Knox, J. B. Cross, V. Bakken, C. Adamo, J. Jaramillo, R. Gomperts, R. E. Stratmann, O. Yazyev, A. J. Austin, R. Cammi, C. Pomelli, J. W. Ochterski, R. L. Martin, K. Morokuma, V. G. Zakrzewski, G. A. Voth, P. Salvador, J. J. Dannenberg, S. Dapprich, A. D. Daniels, O. Farkas, J. B. Foresman, J. V. Ortiz, J. Cioslowski and D. J. Fox, *Gaussian 09*, *Revision A.01*, Gaussian, Inc., Wallingford CT, 2009.
30. J. C. Rienstra-Kiracofe, W. D. Allen and H. F. Schaefer III., *J. Phys. Chem. A*, **2000**, *104*, 9823–9840.